THE JOURNAL OF PHYSICAL CHEMISTRY B

Article

Cite This: J. Phys. Chem. B 2019, 123, 5463−5473

pubs.acs.org/JPCB

Thermodynamic View of Proton Activated Electron Transfer in the Reaction Center of Photosynthetic Bacteria

Péter Maróti*

Institute of Medical Physics, University of Szeged, Rerrich Béla tér 1, Szeged, H-6720, Hungary

ABSTRACT: The temperature dependence of the sequential coupling of proton transfer to the second interquinone electron transfer is studied in the reaction center proteins of photosynthetic bacteria modified by different mutations and treatment by divalent cations. The Eyring plots of kinetics were evaluated by the Marcus theory of electron and proton transfer. In mutants of electron transfer limitation (including the wild type), the observed thermodynamic parameters had to be corrected for those of the fast proton pre-equilibrium. The electron transfer is nonadiabatic with transmission coefficient 6×10^{-4}, and the reorganization energy amounts to 1.2 eV. If the proton transfer is the rate limiting step, the reorganization energy and the works terms fall in the range of 200−500 meV, depending on the site of damage in the proton transfer chain. The product term is 100−150 meV larger than the reactant term. While the electron transfer mutants have a low free energy of activation (∼200 meV), the proton transfer variants show significantly elevated levels of the free energy barrier (∼500 meV). The second electron transfer in the bacterial reaction center can serve as a model system of coupled electron and proton transfer in other proteins or ion channels.

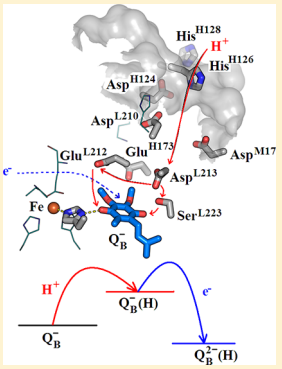

INTRODUCTION

The transfer of electrons and protons in living systems comprise the molecular fundamentals of bioenergetics and many free energy conversion mechanisms.[1,2] The movement of the electrons and protons are often coupled in concerted or sequential fashion[3] and can be accompanied by conformational changes in light- or redox-driven proton pumps of mitochondria[4] and photosynthetic membranes[5] or in radical initiation and transport of biological interest.[6] Despite the recent amazing progress in theory,[7,8] calculations,[9] and experiments,[10] the specific details of electron/proton coupling in biological processes or in model systems of catalysts, fuel cells, solar cells, and chemical sensors remain largely to be resolved. The reaction center (RC) protein of photosynthetic bacteria has been a favorite target of light-induced electron and proton transfer, and these studies allow us now to define how the coupling is manifested.[11−14]

In RC of photosynthetic bacterium *Rhodobacter sphaeroides*, the transfer of electrons is generated by light excitation (flashes) resulting in primary charge separation between the bacteriochlorophyll dimer (P) and the acceptor quinone complex (Q, consisting of primary (Q_A) and secondary (Q_B) quinones): $PQ \Rightarrow P^+Q^-$. Upon subsequent saturating excitations, Q_B performs reduction cycle of period 2 flashes.[11] After the first flash, the first interquinone electron transfer (ET) $Q_A^-Q_B \underset{H^+}{\leftrightarrow} Q_AQ_B^-$ is associated with uptake of substoichiometric amount of H^+ ions.[15] Q_B^- does not bind proton; instead, Glu−L212 is protonated at neutral pH by internal proton-rearrangement, although the (Bohr-) proton is probably distributed over other neighboring residues.[13,16] After the second flash, the second interquinone ET is preceded by uptake of the first (chemical) proton by Q_B:

$$Q_A^-Q_B^- \overset{H^+}{\longleftrightarrow} Q_A^-Q_BH \overset{e^-}{\leftrightarrow} Q_AQ_BH^-$$

followed by uptake of the second (chemical) proton: $Q_AQ_BH^- \overset{H^+}{\longleftrightarrow} Q_AQ_BH_2$. The fully reduced quinol Q_BH_2 is released and replaced by an oxidized quinone. The structural view of the proton delivery pathway to reduced Q_B is shown in Figure 1. The path from the proton entry gate of His−H126 and His−H128 via Asp−L210 and Asp−M17 up to Asp−L213 is shared by both the first and second protons taken up from the cytoplasmic medium.[17] The first H^+ ion is delivered directly to the C1−O group of Q_B^- from Asp−L213 through Ser−L223 and the second proton to Q_B^- from Asp−L213 via Glu−L212. From studies on different mutants, it was possible to estimate the Q^- semiquinone of WT to have a $pK_a \approx 4.5$, quite similar to the value in aqueous solution.[18,19]

A series of former outstanding works[20−22] have provided a convincing description of the second electron transfer whose schematic energetic landscape is depicted in Figure 2.

The (interquinone) transfer of the second electron from Q_A^- to Q_B^- is a proton-activated process as the ET should be preceded by the uptake of the first proton $Q_A^-Q_B^- \leftrightarrow Q_A^-Q_BH$. The proton pre-equilibrium sets the stage for the electron transfer: $Q_A^-Q_BH \rightarrow Q_AQ_BH^-$. The proton and electron transfer steps are consecutive processes. The rates can be conveniently modified either by mutations directed to specific amino acids at key positions[23−25] or by divalent cations.[26,27] Depending on which transfer becomes the rate

Received: April 14, 2019
Revised: June 3, 2019
Published: June 10, 2019

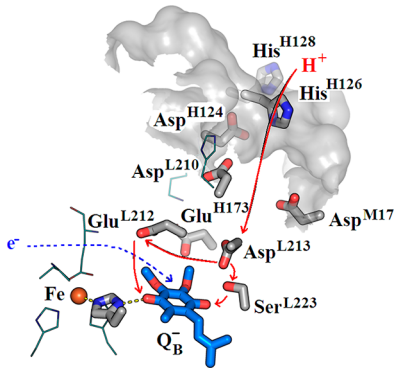

Figure 1. Coupling of stepwise proton uptake (H^+) and reduction (e^-) of Q_B^- in the Q_B site of buried acid cluster in RC of photosynthetic bacteria. The proton entry site (surface histidines) and the approximate pathway, via several carboxylates, are labeled by residue number. The path bifurcates at AspL213 to deliver H^+ to the two carbonyls via SerL223 (first proton) and GluL212 (second proton). The electron is observed to arrive from Q_A^- after the first H^+ uptake. The gray contoured surface encloses the surface of the RC. The figure was prepared in VMD; structure file was 1dv3.pdb.

limiting step, electron transfer (ET) (including wild type, WT) or proton transfer (PT) variants can be distinguished.[11,16] In electron transfer mutants, the pre-equilibrium protonation is energetically unfavorable but is fast; therefore, the electron transfer remains the bottleneck of the observed kinetics. However, the roles are swapped in proton transfer mutants: the protonation is much slower than the subsequent electron transfer and controls the observed kinetics. As the protonation becomes the rate limiting step, the kinetics of the second electron transfer will show a deuterium isotope effect.[18]

To understand this reaction fully, it is necessary to digest not just the kinetics but also the thermodynamics that reveals the energy levels, as well as the driving forces of the electron/proton transfer. The driving force (the Gibbs free energy) of the reaction is composed of enthalpic and entropic components reflecting different components of the energetics of the reaction. In contrast to the kinetics of the transfer mechanisms, the thermodynamic information is far less available. However, with a proper understanding of the kinetic mechanism, we would expect to make some headway with the fundamental thermodynamics of the proton coupled second electron transfer and would hope to describe the kinetic model with some essential quantitative detail. On the other hand, experiences with charge separation, recombination and first interquinone electron transfer might temper our expectations. Photoacoustic,[28−30] delayed fluorescence,[31] and lipid[32] studies revealed serious challenges of the existing notions for the enthalpy and entropy contributions in the free energy changes of the reactions $P^* \leftrightarrow P^+Q_A^- \leftrightarrow P^+Q_AQ_B^-$.

In this work, the temperature dependence of the second ET is characterized in RCs of wild type (WT), treated by divalent cations and of various (electron or proton transfer limited) mutants to obtain enthalpy and entropy contributions to the activation energy. The analysis based on the Marcus theory is used not only for electron transfer (ET mutants) but for

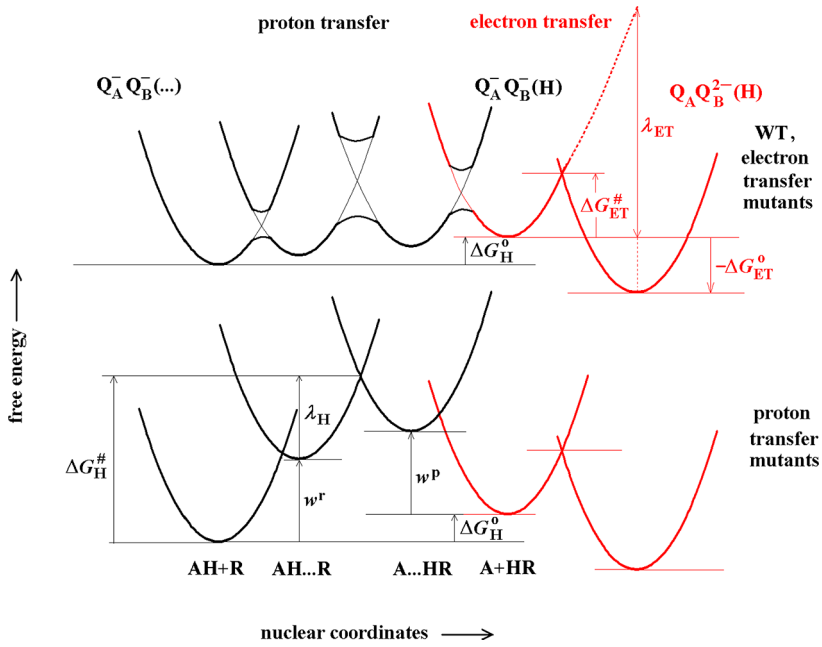

Figure 2. Landscape of the standard free energy of the states (subscript o) participating in the stepwise proton (black, H) and electron (red, ET) transfer vs nuclear coordinates showing the activation free energies (subscript #) and works terms (w) during the second interquinone electron transfer in bacterial RC. The reactant and product surfaces are represented as parabolas. In wild type (WT) and electron transfer mutants, the unfavorable (uphill) proton transfer is very fast with very small activation energies on the adiabatic surface of the protonable groups compared to those of the subsequent electron transfer (upper panel). At each intersection point of the proton transfer, the reactant (initial) and product (final) states interact strongly (V_{if}) resulting in the large separation of the two curves by $2V_{if}$ (adiabatic transfer). However, the electron transfer is nonadiabatic, and the splitting is very small at the crossing. The reorganization energy, λ_{ET}, is given by the position on the reactant curve that lies above the equilibrium coordinate of the product curves. In proton transfer mutants, the rate of the proton transfer becomes the bottleneck due to a defect in the bucket brigade mechanism while the thermodynamics of the electron transfer does not change (lower panel). The protonation of the residue R next to the defect is rescued by a bound protonated acid (AH). The formation of the activated complex from the reactants and dissociation of the products involves works terms, w^r and w^p, which raise the reactant and product curves by different amounts.

DOI: 10.1021/acs.jpcb.9b03506
J. Phys. Chem. B 2019, 123, 5463−5473

proton transfer (PT mutants) by inclusion of works terms. The activation energy parameters are consistent with reasonable values for the reorganization energy of the ET in electron transfer mutants and for the works terms of the proton transfer in proton limited mutants.

MATERIALS AND METHODS

The design and techniques of molecular engineering to produce mutant RCs from nonsulfur photosynthetic bacterium *Rba. sphaeroides* were described earlier.[33−35] The RCs were solubilized from membrane fragments (chromatophores) by ionic detergents lauryl (dodecyl) dimethylamine-*N*-oxide (LDAO) followed by purification by ammonium sulfate and DEAE-Sephacel column[15] to a purity OD_{280}/OD_{800} of 1.3. The aggressive LDAO detergent was exchanged with nonionic Triton X-l00 detergent by overnight dialysis.

The secondary Q_B activity was reconstituted by addition of excess ubiquinone-10 solubilized in ethanol to the RC ([UQ]/[RC] > 10). The degree of reconstitution was assayed by the ratio of the amplitudes of the slow and fast phases of the charge recombination kinetics detected at 430 nm. The measurement of the kinetics of the second electron transfer, $Q_A^- Q_B^- \rightarrow Q_A Q_B H^-$ was described earlier.[18,19] The absorption change induced by the second of two short saturating flashes 0.5 s apart was detected at 450 nm. The rereduction of P^+ by exogenous electron donor should take place before the second flash. Depending on the kinetic conditions, the appropriate electron donor should be selected. Although the reduced cytochrome-c^{2+} (horse heart grade VI, reduced (>95%) by hydrogen gas on platinum black) is a fast electron donor to P^+ (oxidation halftime <100 μs), the complex kinetics of cytochrome oxidation can extend to a larger time range (~1 ms) where it may overlap that of the electron transfer. The ethanolic solutions of ferrocene at large (150−200 μM) concentrations are also fast donors (halftime ~2 ms), but ethyl ferrocene or dimethyl ferrocene at low (2−4 μM) concentration reduce P^+ with a halftime of 200−500 ms, which is still significantly faster than that of the charge recombinations. A mixture (2−2 mM each) of buffers (citric acid, Mes, Mops, Pipes, Tris, Ches, and Caps in the order of increasing pK_a values) were used to stabilize the pH of the solution. The second electron transfer was efficiently inhibited by addition of stoichiometric amount of divalent cations (Cd^{2+} or Ni^{2+}).[11,26,27]

RESULTS

Free Energies of Activation. For a wide range of electron and proton transfer mutants, the rates of the second electron transfer $k^{(2)}_{AB}$ were measured in the physiological temperature range. From the observed temperature-dependence of the rate constant, the activation free energy ($\Delta G_0^{\#}$) of the rate limiting step can be obtained. The kinetic bottleneck can be either the proton equilibration or the electron transfer. The thermodynamically related Eyring rate equation for the activated complex state (transition state theory) describes the correlation between the free energy barrier and the reaction rate:

$$k_{AB}^{(2)} = \kappa \cdot \frac{k_B T}{h} \cdot \exp\left(-\frac{\Delta G_o^{\#}}{k_B T}\right) \quad (1)$$

Here κ is a transmission coefficient, k_B is the Boltzmann constant, T is a temperature, and h is the Planck constant. By using the relationship between the changes of the free energy $\Delta G_0^{\#}$, enthalpy $\Delta H_0^{\#}$ and entropy $\Delta S_0^{\#}$ of activation: $\Delta G_0^{\#} = \Delta H_0^{\#} - T\cdot\Delta S_0^{\#}$, the plot of $\ln(k^{(2)}\cdot h/(k_B T))$ versus $1/k_B T$ should deliver straight line (Eyring plot) with slope of $-\Delta H_0^{\#}$ and intercept of $[\ln(\kappa) + \Delta S_0^{\#}/k_B]$. The observed thermodynamic energies characterize the need of energy to the activated state of the corresponding rate-limiting step of the proton or electron transfer. More specifically, the enthalpy change of activation ($\Delta H_0^{\#}$) relates to the height of the energy barrier of the activated-state complex, and the entropy change of activation ($\Delta S_0^{\#}$) refers to the thermodynamic probability, i.e. the ratio of the numbers of available configurations in the activated complex and in the reactant states. However, the true entropy change $\Delta S_0^{\#}$ does not come directly from the interception in the Eyring (transition state) representation but from the degree of adiabaticity of the (electron) transfer, κ that should also be taken into account (discussed later).

Figure 3 demonstrates the linear relationship for RCs typical of electron transfer (WT and M17DN single mutant) and of proton transfer (WT + 1 mM Ni^{2+}) limitation of the second ET. The statistical errors of the derived parameters in a given sample and the biological errors (the standard deviations relative to the means in several (typically 3−4) samples) are in the range of 10−15%. Large changes in slope (enthalpy of activation) and vertical position (free energy change of activation or rate constant of the second ET) can be observed. The thermodynamic parameters were determined from the measured temperature-dependence of the rates by least-squares linear fit using eq 1 for a wide variety of single and double mutants and divalent cation (Cd^{2+} and Ni^{2+}) treated RCs in a similar way as exposed in Figure 3. The derived energetic quantities were tabulated both for electron transfer (Table 1) and for proton transfer limited variants (Table 3) at pH 7.5. Additionally, the free energy of activation and its

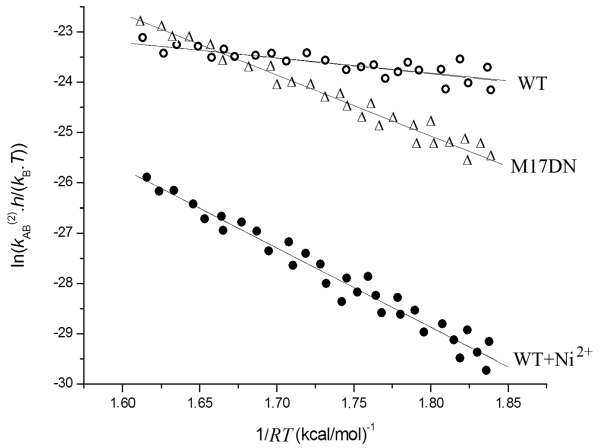

Figure 3. Temperature-dependence of the observed rate constant of the second electron transfer ($k_{AB}^{(2)}$) in RCs limited by ET (WT and M17DN single mutant) or by PT (WT+ Ni^{2+}) in Eyring plot representation (see eq 1 and R is the universal gas constant). The temperature was changed in the physiological range between 4 and 40 °C. The enthalpy and entropy changes of the activation were determined from the slopes and intersections of the fitted straight lines and collected together with those of other similar RC variants in Tables 1−3. Conditions: 4 μM RC, 0.02% TX, 40 μM UQ_{10}, 3−3 mM Mops and Tris, pH 7.5, 20 μM cyt c (M17DN) or 6 μM dimethyl ferrocene (WT) or 500 μM ethyl ferrocene (WT + 1 mM $NiCl_2$).

DOI: 10.1021/acs.jpcb.9b03506
J. Phys. Chem. B 2019, 123, 5463−5473

Table 1. Components of Activation Parameters for the Observed Second Electron Transfer (Total), for the Proton Pre-Equilibrium (H) and for the True Electron Transfer (ET) in Electron Transfer Mutants at pH 7.5 (in meV)

	observed[a]				proton pre-equilibrium[c]			electron transfer[d]		
strain	$\Delta H^{\#}_{tot}$	$T{\cdot}\Delta S^{\#}_{tot}$	$\Delta G^{\#}_{tot}$	pK_R[b]	$\Delta H^{o\prime}_{H}$	$T{\cdot}\Delta S^{o\prime}_{H}$	$\Delta G^{o\prime}_{H}$	$\Delta H^{\#}_{ET}$	$T{\cdot}\Delta S^{\#}_{ET}$	$\Delta G^{\#}_{ET}$
WT	200	−180	380	4.5	−90	−260	170	290	80	210
M17DN	550	120	430	3.8	−90	−310	220	640	430	210
L210DN	520	90	430	3.8	−90	−310	220	610	400	210
H173EQ[e]	410	− 60	470	3.5	−90	−330	240	500	270	230

[a]From temperature dependence of the measured rate of the second ET, $\kappa = 6 \times 10^{-4}$ [b]pK_R refers to the proton accepting carboxyl residue or Q_B^-/Q_B^-(H) itself. [c]Data from oxy-acids [d]Calculated from eq 2 [e]H173EQ may be partially PT-limited[34]

enthalpic and entropic components demonstrate weak pH-dependence both for ET (Table 2) and PT (Table 3) mutants.

Thermodynamics of Acid Dissociation and Association. Whatever rate model is used for the rate-limiting electron transfer (ET), the proton pre-equilibrium (acid association) parameters ($\Delta G^{o\prime}_{H}$, etc) combine with those of the true activation step ($\Delta G^{\#}_{ET}$, etc) to give the observed or total activation energetics ($\Delta G^{\#}_{obs}$, etc) as follows:

$$\Delta G^{\#}_{obs} = \Delta G^{o\prime}_{H} + \Delta G^{\#}_{ET}$$
$$\Delta H^{\#}_{obs} = \Delta H^{o\prime}_{H} + \Delta H^{\#}_{ET}$$
$$T{\cdot}\Delta S^{\#}_{obs} = T{\cdot}\Delta S^{o\prime}_{H} + T{\cdot}\Delta S^{\#}_{ET} \quad (2)$$

Unfortunately, the thermodynamic parameters of the proton equilibrium of the terminal proton acceptor semiquinone in the RC cannot be measured directly. However, the acid association/dissociation values can be estimated by use of the dissociation heats of oxy-acids of different pK_a values.[36] There is a strong linear correlation between pK_a and the enthalpy change $\Delta H^{o\prime}_{H}$ (and hence also $T{\cdot}\Delta S^{o\prime}_{H}$, because pK_a is linear with $\Delta G^{o\prime}_{H}$) (Figure 4).

Most of the commonly encountered acids are oxy-acids containing the structure X−O−H, where the central atom X can be connected to other atoms or atom groups. As the acidic hydrogen is bound to an oxygen atom, the bond strength (length) is not an issue due to the binary nonmetal hydrides. More exactly, the electronegativity of the central atom X relative to the surrounding atoms in the molecule and the number of O atoms around X determines the oxy-acid acidity (pK_a). The measured dissociation heat for a number of oxy-acids shows a strong linear correlation with the pK_a and the plot allows one to interpolate the changes of the enthalpy change of dissociation and association for an oxy-acid with pK_a = 4.5 (that would correspond to a carboxyl acid in the proton delivery chain and/or to Q_B^- itself) at pH = 0. The thermodynamic quantities are $\Delta G_H^\circ = 2.303{\cdot}RT{\cdot}pK_a$ = +6.0 kcal/mol, ΔH_H° = +1.76 kcal/mol and $T{\cdot}\Delta S_H^\circ$ = −4.24 kcal/mol (dissociation) and $\Delta G_H^\circ = -2.303{\cdot}RT{\cdot}pK_a$ = −6.0 kcal/mol, ΔH_H° = −1.76 kcal/mol and $T{\cdot}\Delta S_H^\circ$ = +4.24 kcal/mol (association). The actual (relevant) values of oxy-acid association at pH = 7.5 should be calculated from the standard values: $\Delta G^{o\prime}_{H} = -2.303{\cdot}RT{\cdot}(pK_a - pH)$ = +4.02 kcal/mol = 170 meV, $\Delta H^{o\prime}_{H} = \Delta H_H^\circ$ = −1.76 kcal/mol = −76 meV and $T{\cdot}\Delta S^{o\prime}_{H} = T{\cdot}\Delta S_H^\circ - 2.303{\cdot}RT{\cdot}pH$ = −5.81 kcal/mol = −252 meV.

Driving Force Assay of PT Mutants. The damaged proton transfer route to Q_B in PT mutants can be partly recovered by rescue agents, which bind to the RC and ensure H^+ ions and proper electrostatics for the transfer.[16,35,37] Due to the proton limitation of $k^{(2)}_{AB}$, the rate of recovery will depend on the difference of pK_a of the rescuing acids (proton donor) and pK_R of the carboxyl group in the chain (proton acceptor). The monomolecular rate constant of the proton transfer, $k^{(2)}_{AB}$ is the product of the observed bimolecular rate constant $k_{(2)}$ and the dissociation constant of the rescuing agent K_D: $k^{(2)}_{AB} = K_D{\cdot}k_{(2)}$.[35]

Figure 5 demonstrates the results of a driving force assay carried out in three different PT mutants where the damage in the chain of protonatable residues was further and further from the protein surface (closer and closer to the terminal proton acceptor Q_B^-): H126HA/H128HA, L210DN/M17DN, and L213DN.[16] A limited range of driving force (the standard free energy of the reaction) would yield a close to linear relationship with the logarithm of the rates of proton transfer reactions (and hence the activation free energy). However, the measured rates on a more extended free energy range exhibit significant curvature and fit well to a quadratic relationship. The deviation from the straight line is not due to limitation of the diffusion, as the bimolecular rate constants of proton transfer in these RC mutants are significantly smaller than the upper limit of the rate constant associated with aqueous proton diffusion $k_{max} = 1.4 \times 10^{11}$ $M^{-1}{\cdot}s^{-1}$.[38]

DISCUSSION

Marcus Analysis of the WT and ET Mutants. The kinetic data of the second ET were analyzed by Eyring plots. To obtain the true activation parameters for the rate limiting ET, both the nonadiabaticity of the ET described by the Marcus theory[39] and the thermodynamics of the proton pre-equilibrium should be taken into account.

The maximum rate of ET can be estimated from EPR experiments referring to exchange coupling in the semiquinone biradical $Q_A^{\bullet-}Q_B^{\bullet-}$[40] and from kinetic measurements:[41] $k_{max} = 3.5 \times 10^9$ s^{-1}. On the basis of this value, the transmission coefficient (adiabaticity parameter) can be calculated from eq 1: $\kappa = k_{max}{\cdot}h/(k_BT) \approx 6 \times 10^{-4}$. This means that κ is very far from 1 for WT (and electron transfer mutants) indicating a very small interaction energy between the electron donor and acceptor (see the crossing of the parabolas in Figure 2). Therefore, the rate limiting step of $k^{(2)}_{AB}$ in WT is the nonadiabatic electron transfer with small κ value.

Due to the highly nonadiabatic nature of the ET, the determination of the true entropy change of the ET from the observed data requires modification both for proton equilibrium and for (ln κ). In the wild type (ET-limited) RC, the rapid protonation pre-equilibrium contributes "normally" to the net activation parameters, with a negative standard enthalpy, ΔH_H° = −1.76 kcal/mol = −76 meV, a positive standard entropy, $T{\cdot}\Delta S_H^\circ$ = +4.24 kcal/mol = +184 meV and a negative entropy of mixing as the pH increases ($-2.303{\cdot}RT{\cdot}pH$), so that $T{\cdot}\Delta S^{o\prime}_{H}$ = −5.81 kcal/mol = −252

DOI: 10.1021/acs.jpcb.9b03506
J. Phys. Chem. B 2019, 123, 5463−5473

Table 2. pH-Dependence of the Observed Activation Parameters of the Second ET and of the True Activation Energies of the Electron Transfer in Some ET-Limited RCs (in kcal/mol)

	observed[a]			proton pre-equilibrium[b]			electron transfer[c]		
strain	$\Delta(\Delta H^{\#}_{tot})/\Delta(pH)$	$\Delta(T{\cdot}\Delta S^{\#}_{tot})/\Delta(pH)$	$\Delta(\Delta G^{\#}_{tot})/\Delta(pH)$	$\Delta(\Delta H^{o\prime}_{H})/\Delta(pH)$	$\Delta(T{\cdot}\Delta S^{o\prime}_{H})/\Delta(pH)$	$\Delta(\Delta G^{o\prime}_{H})/\Delta(pH)$	$\Delta(\Delta H^{\#}_{ET})/\Delta(pH)$	$\Delta(T{\cdot}\Delta S^{\#}_{ET})/\Delta(pH)$	$\Delta(\Delta G^{\#}_{ET})/\Delta(pH)$
WT	+0.39	−0.30	+0.69	0	−1.33	+1.33	+0.39	+1.03	−0.64
M17DN	+2.0	+1.47	+0.52				+2.0	+2.80	−0.81
L210DN	+2.0	+1.45	+0.55				+2.0	+2.78	−0.78
H173EQ	+1.81	+0.95	+0.86				+1.81	+2.28	−0.47

[a]From temperature dependence of the measured rate of the 2nd ET. [b]Data from oxy-acids. The data refer to all strains. [c]Calculated from eq 2

meV at pH 7.5. From the measured values $\Delta G^{\#}_{obs}$ = 8.7 kcal/mol = 380 meV, $\Delta H^{\#}_{obs}$ = 4.5 kcal/mol = 200 meV, and $T{\cdot}\Delta S^{\#}_{obs}$ = −4.2 kcal/mol = −180 meV and eqs 2, we then find that the ET step has $\Delta G^{\#}_{ET}$ = +4.68 kcal/mol = 200 meV, $\Delta H^{\#}_{ET}$ = +6.26 kcal/mol = 270 meV, and $T{\cdot}\Delta S^{\#}_{ET}$ = +1.61 kcal/mol = 70 meV.

The resulting value of free energy change of activation of the ET, $\Delta G^{\#}_{ET} \approx 200$ meV gives very good correspondence with expectations from Marcus theory for an ET reaction with $\Delta G^{o\prime}_{ET} \approx -250$ meV and $\lambda_{ET} \approx 1200$ meV, i.e., from $\Delta G^{\#}_{ET} = [(\Delta G^{o\prime}_{ET} + \lambda_{ET})^2/(4{\cdot}\lambda_{ET})]$ and $\Delta G^{o\prime}_{ET} = -\lambda_{ET} \pm 2{\cdot}\sqrt{(\lambda_{ET}{\cdot}\Delta G^{\#}_{ET})}$. It should be noted that these relationships are quite sensitive—at least, insofar as we have a narrow range of $\Delta G^{o\prime}_{ET}$ to fit. Even using temperature-dependent measurements, the separation of $\Delta G^{o\prime}_{ET}$ and λ_{ET} is a challenge, as their sum controls the rate coefficient in the Marcus equation.

The $\lambda_{ET} \approx 1.2$ eV for the reorganization energy of the second interquinone ET fits to the wide range of values derived from Dutton's parametrization[42,43] (≈ 800 meV) to molecular dynamics simulations[44] (≈4 eV). It is in the range of typical solvent reorganization energies for ET reactions in solution. The intramolecular electron transfer to the heme from Ru derivates attached near the surface of cytochrome-*c* involves reorganization energies in the range of 600 to 1200 meV.[45] In chromatophores of *R. sphaeroides*, the transfer of the first electron in quinol oxidation by the cytochrome bc_1 complex showed relatively high activation energy (680 meV) and reorganization energy (2.5 eV) that were unexpected from Marcus theory and the short (≈ 7 Å) distances from the structures.[46] The anomaly was interpreted by a mechanism in which the electron transfer was controlled by coupled transfer of the proton. The temperature-dependencies of $P^+Q_A^-$ → PQ_A charge recombination in bacterial RCs with an altered primary acceptor[47,48] or with modified P/P^+ midpoint potentials[49,50] or under electric field modulation[51] were associated with λ_{ET} ranging from ≈600 meV at cryogenic temperature to ≈900 meV at room temperature. A much smaller reorganization energy (≈ 100−200 meV) was simulated for the primary charge separation reactions in RC in accordance with the fast and nearly temperature-independent kinetics of the charge separation.[52] The analogous $P^+Q_B^-$ → PQ_B electron transfer has significantly larger reorganization energy of λ_{ET} = 1300 meV measured at room temperature.[48] The larger reorganization energy of charge recombination from Q_B than that from Q_A reflects probably the fact that the Q_A and Q_B electron carriers are only partially buried in the hydrophobic core of the RC, which is surrounded by a small belt of detergents in the aqueous phase. In addition, the charges of Q_A^- and Q_B^- are not delocalized over large π-electron systems as those of BChl dimer and monomers and BPheo which participate in the early steps of charge separation. The closer localization of π-electrons on quinones makes the electric fields acting on the surrounding amino acid residues relatively strong.

A similar increase of λ_{ET} can be observed if the reorganization energies of the first and second interquinone ETs are compared. While 930,[53] 850,[54] and 760 meV[55] values were reported at room temperature for the $Q_A^-Q_B \rightarrow Q_AQ_B^-$ reaction, we obtained 1200 meV for the reorganization energy of the second $Q_A^-Q_BH^- \rightarrow Q_AQ_B^{2-}H$ electron transfer. The larger value is not out of the line for Q_B-involved reactions in RCs and indicates the more intense interactions of Q_B with protein backbone dipoles or bound water dipoles than Q_A.

DOI: 10.1021/acs.jpcb.9b03506
J. Phys. Chem. B 2019, 123, 5463−5473

Table 3. Observed (Total) Thermodynamic Parameters of Protonation Mutants: Enthalpy, Entropy, and Free Energy of Activation at pH 7.5 and Their pH-Dependence (in kcal/mol)[a]

strain/mutant	$\Delta H^{\#}_{tot}$	$T{\cdot}\Delta S^{\#}_{tot} + RT{\cdot}\ln\kappa$	$\Delta G^{\#}_{tot}$	$\Delta(\Delta H^{\#}_{tot})/\Delta(pH)$	$\Delta(T{\cdot}\Delta S^{\#}_{tot})/\Delta(pH)$	$\Delta(\Delta G^{\#}_{tot})/\Delta(pH)$
WT + Cd	9.6	−1.2	10.8	1.33	+0.41	0.92
WT + Ni	16.6	+4.8	11.8	2.42	+1.41	1.0
M17DN + Cd	13.2	+1.7	11.5	3.61	+2.42	1.19
M17DN + Ni	12.0	+1.0	11.0	1.84	+0.74	1.10
L210DN + Cd	10.4	−1.0	11.4	2.96	+2.32	0.64
L210DN + Ni	15.0	+3.3	11.7			
L210DN/M17DN	15.8	+4.5	11.3	0.78	−0.04	0.82
H173EQ + Cd	14.2	+2.8	11.4			
H173EQ + Ni	17.3	+5.3	12.0			
L213DN (pH = 4.8)	11.2	−0.8	12.0	0.25	−0.92	1.16
L213DN/M44ND	16.0	+6.3	9.7			
L213DN/M44ND + Cd	15.6	+4.7	11.7			
L213DN/M44ND + Ni	16.4	+4.7	11.7	1.73	+0.88	0.84

[a]The entropy term is determined by the transmission term, κ.

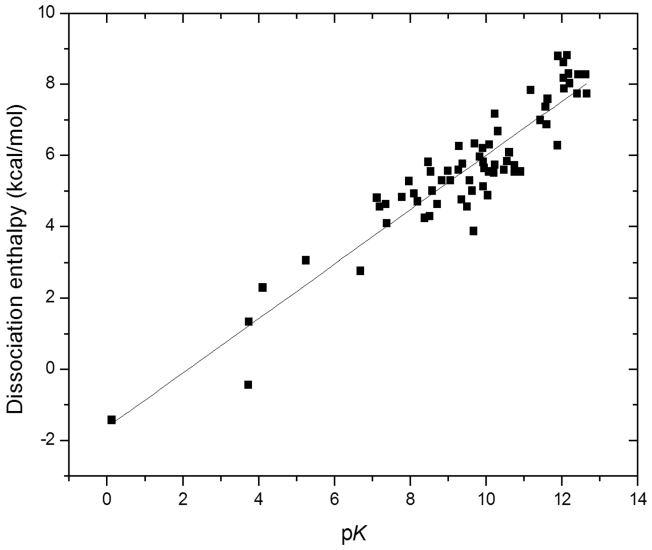

Figure 4. Oxy-acid dissociation heats vs pK_a at pH = 0 (data taken from ref 36). The best fit straight line for the standard enthalpy change is ΔH° = (0.7561·pK_a − 1.6401) kcal/mol.

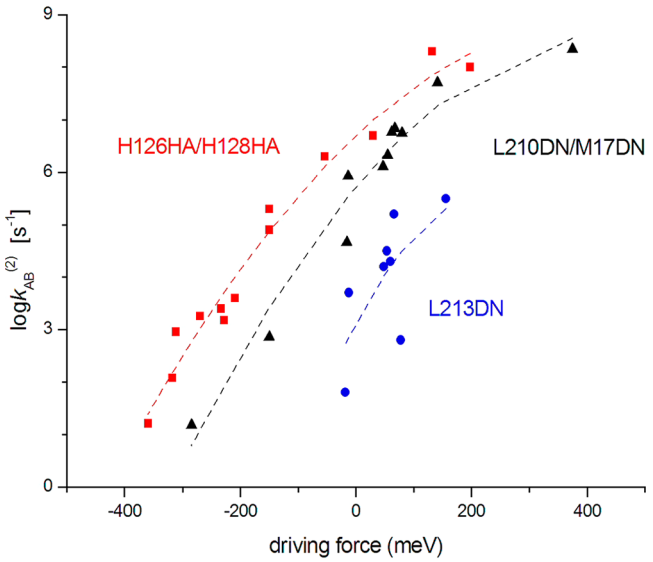

Figure 5. Marcus plots of the second electron transfer rates ($k_{AB}^{(2)}$) for rescue of proton limited mutants (H126HA/H128HA,[35] L210DN/M17DN,[37] and L213DN) by acids. The $k_{AB}^{(2)}$ values were derived from the bimolecular rate constants $k_{(2)}$ of the chemical rescue mutants by $k_{AB}^{(2)} = K_D \cdot k_{(2)}$ where K_D was the dissociation constant of the rescuing acids (~10 mM for amine-containing acids and ~1 M for small acids). The driving force of the proton transfer was calculated from the difference of pK values between the proton accepting carboxyl group (pK_R = 4.5) and proton donating acid (pK_A): 60 meV·(pK_R − pK_A). The fitted curves (dashed lines) to the data were calculated from the Marcus rate theory for protons (eq 1 (eq 4)), and the parameters are given in Table 4.

Additionally, the increase of λ_{ET} of the second ET relative to that of the first ET suggests that even slight alteration of the redox forms or possible displacement of Q_B may result in significant difference of the interactions with the surroundings.

Marcus Analysis of the Proton Transfer Mutants. The communication between the aqueous bulk phase and Q_B^- is mediated by a chain of protonatable amino acids (Figure 1) which assures very fast proton transport. The exchange of an active proton carrier to a nonionizable residue by mutation or disruption of the pathway by divalent cations at the proton gate can be catastrophic as the rate of proton delivery drops tremendously and becomes the rate limiting step of the second electron transfer. Rescuing acids, however, can largely restore the destroyed step in the bucket-brigade mechanism. The chemical rescue appears to conform to a Marcus analysis because it is a two-state system of donor (AH) and acceptor (R) groups with relatively closely matched pK_as. As R can be a carboxylic acid (or Q_B^- itself) for which p$K_a \approx 4.5$ has been estimated[12,18,19] (see Table 1), ΔpK_a is in the ballpark of ±3. We expect that the Marcus analysis would give meaningful parameters for the thermodynamics of the proton transfer in proton limited mutants.

As the Marcus theory describes a wide range of charge transfer processes including proton transfer, it can be used to analyze the relation between the rates and driving force provided by Figure 5. According to the Marcus rate theory applied to proton transfer,[56,57] the overall activation energy $\Delta G^{\#}$ can be expressed by the standard free energy of reaction with the required active site conformation ΔG°_R and by the intrinsic energy barrier (reorganization energy) λ_H:

DOI: 10.1021/acs.jpcb.9b03506
J. Phys. Chem. B 2019, 123, 5463−5473

$$\Delta G^{\#} = w^{r} + \lambda_{H}\cdot\left(1 + \frac{\Delta G^{o}_{R}}{4\lambda_{H}}\right)^{2} \quad (3)$$

The free energy of activation is extended by a works term w^{r} that is independent of the driving force and constitutes the constant part of the energy barrier as it does not change on the driving force. Its introduction has practical and empirical importance: it represents the part of the free energy of activation that must be subtracted from $\Delta G^{\#}$ to be able to fit the observed free energy of activation to the Marcus equation. The reorganization energy is the value of the apparent activation energy ($\Delta G^{\#} - w^{r}$) at zero standard driving force ($\Delta G^{\circ}_{R} = 0$). It consists of two reorganization terms: the energies for intramolecular and for solvent reorganizations. The intramolecular reorganization is determined by the bond-length change between donor or acceptor and proton, and the solvent reorganization is defined by the donor−acceptor distance and properties of the medium.

The standard free energy of reaction ΔG°_{R} of the required conformation is related to the observed overall free energy for the reaction by works terms: $\Delta G^{\circ} = w^{r} + \Delta G^{\circ}_{R} - w^{p}$. After insertion into eq 3, we obtain

$$\Delta G^{\#} = w^{r} + \lambda_{H}\cdot\left(1 + \frac{\Delta G_{o} + w^{p} - w^{r}}{4\lambda_{H}}\right)^{2} \quad (4)$$

The works terms w^{r} and w^{p} include the electrostatic energy of attraction of the reagents and repulsion of the products, respectively. More specifically, w^{r} and w^{p} represent the energies of catalysis in the dehydration direction and in the reverse direction, respectively. In the case of nonenzymatic bimolecular proton transfer reactions, these work functions were introduced to measure the energy requirement to align acceptor, donor, and surrounding water for facile proton transfer.[57] This concept has been extended into enzymatic systems.[58,59] If ΔG° is large, the influence of w^{r} and w^{p} will be small and they are usually neglected. In biological ET, the cofactors are often preorganized, and the works terms are properly absent. In proton transfer, however, this is not necessarily the case.

The observed curvature in the plot of the logarithm of the rate of proton transfer versus the driving force predicts the validity of the Marcus free energy relation and indicates that the Marcus theory can account for the kinetics of proton transfer in bacterial RC mutants where the proton transfer is the rate liming step in the second electron transfer (Figure 5). Moderately high intrinsic barriers ($\lambda_{H} \sim 100-350$ meV) and works terms ($w \sim 200-500$ meV) were measured, and the works term w^{p} was always larger than w^{r} ($w^{p} - w^{r} \approx 100$ meV) (Table 4). In agreement with Hammond's postulate for the endergonic reaction, the transition state is closer to the product than to the reactant state (the peak ($\Delta G^{\#}_{obs}$) is not at the same position on the two adiabatic surfaces, Figure 2. The structure of the transition state resembles the products (A···HR) more than the reactants (AH···R). This type of comparison is useful because the transition state of proton transfer is difficult to characterize experimentally. The free energy of the transition state and that of the product are changing parallel in the endothermic reaction: higher energy transition state leads to higher energy product. Indeed, both $\Delta G^{\#}_{obs}$ and ΔG°_{obs} increased ($\frac{\Delta(\Delta G^{\#}_{tot})}{\Delta(pH)} > 0$) upon increase of the pH for all PT mutants (Table 3).

Table 4. Marcus Theory Parameters of the First Proton Uptake in Proton Transfer Mutants of Bacterial RCs[a]

proton transfer mutants	intrinsic barrier $\Delta G^{\#}_{o}$ (meV)	Works functions w^{r} (meV)	Works functions w^{p} (meV)
H126HA/H128HA[b]	350	170	240
L210DN/M17DN[c]	290	180	340
L213DN	100	360	500

[a]Data were obtained by least-squares fit of eq 4 to rate constants for intramolecular proton transfer $k_{AB}^{(2)}$ given in Figure 5. The transmission coefficient is at the adiabatic limit: $\kappa \approx 1$. [b]Data from ref 37 [c]Data from ref 35

In various gramicidin A channels, the Gibbs free energies of activation ($\Delta G^{\#}_{o}$) for protons are within the range of 280−300 meV in GMO (glycerylmonooleate) bilayers and of 210−230 meV in DiPhPC (diphytanoylphosphatidylcholine) bilayers.[60] In human carbonic anhydrase enzyme, similarly low intrinsic barrier and works terms (430 meV) were measured for proton transfer from a donor to a zinc-bound hydroxyl within the active site of the enzyme as we observed in bacterial RC.[59] Once the donor and acceptor are in position for proton transfer (e.g., along a preformed hydrogen bond), the intrinsic barrier for nonenzymatic proton transfer between similar groups is quite low ($\lambda_{H} \sim 40$ meV). If the process of simple bimolecular proton transfer involves an intervening water molecule, the apparent intrinsic barrier is higher, typically about 200 meV. However, calculations of individual, pair wise PTs resulted in much larger values of $\lambda_{H} \approx 3$ eV with negligible works terms, indicating the very small demand of energy to arrange the water molecules for adequate function.[61] It supports the conclusion, that long-range PT in bacterial RC must consists of several, essentially adiabatic ($\kappa \approx 1$) steps and not of nonadiabatic, two-state steps as in ET.[1]

Our findings show that both the intrinsic kinetic barriers and the works functions for proton transfer mutants in bacterial RC are high compared to those with bimolecular, nonenzymic proton transfers in solutions. These thermodynamic values answer the question of why proton transfer in these RC mutants is significantly slower than the upper limit of rate constant associated with aqueous proton diffusion[38] $k_{max} = 1.4 \times 10^{11}$ $M^{-1}\cdot s^{-1}$.

pH-Dependence of the Activation Parameters. The enthalpy and entropy contribution of the free energy of activation ($\Delta G^{\#} = \Delta H^{\#} - T\cdot\Delta S^{\#}$) and their pH-dependence are also highly informative characteristics of the thermodynamics of the PT coupled ET. The observed (total) free energy of activation and the enthalpy and the entropy components are plotted in Figure 6 for WT and all mutants used in this study. By having the smallest observed free energy, enthalpy, and entropy of activation, the WT is located at a well separated position in the 3D space of the thermodynamic parameters. As often observed in uncatalyzed chemical reactions in aqueous solution,[62] the WT and a few mutated (H173EQ) and Cd^{2+}-treated (WT, L210DN and M17DN) RCs show negative activation entropy, which adds a penalty ($-T\cdot\Delta S^{\#}$) to the overall activation free energy. Such an entropy demand is most often considered as sign of a loss of freedom of the reactants as they pass through their transition state. All the other electron transfer and proton transfer mutants used in this study are characterized by high values of observed activation free energy. It is due to the dramatic

DOI: 10.1021/acs.jpcb.9b03506
J. Phys. Chem. B 2019, 123, 5463−5473

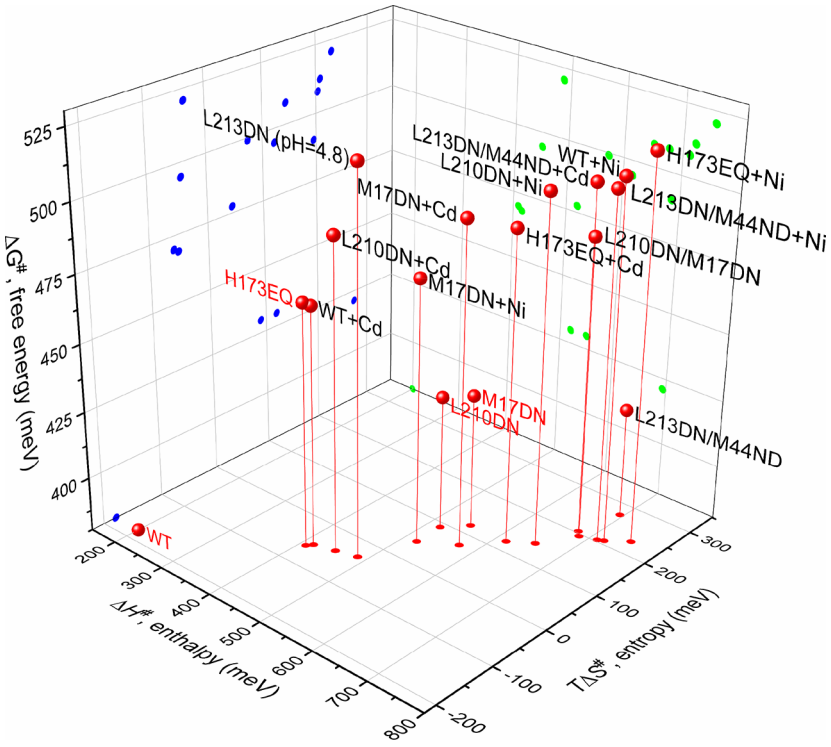

Figure 6. 3D plot of the components of the observed activation energy in WT and RCs modified chemically (divalent cations, Cd^{2+} and Ni^{2+}) or by mutations (single (H173EQ, L210DN, M17DN, and L213DN), double (L210DN/M17DN), and revertant (L213DN/M44ND)) or both. The RCs of electron transfer limitation are marked by red and those of PT limitation by black. Note the considerable separation of WT from ET and PT mutants.

increase of the enthalpy of activation (e.g., changes of the chemical bonds, desolvation, or electrostatic and conformational strains) which is only partially compensated by smaller increase of the entropy. The loss of entropy involved in the transition state (see WT) is overshadowed by other factors both in the RC and in the surrounding medium leading to entropy increase in these mutants. Some enzymes show very large entropy increases: the extremely high rates of GTP hydrolysis on the ribosome, for example, are explained by the exceptionally large increase of entropy of activation.[63]

The observed activation energy is the combination of those of the true (ET and PT) and proton pre-equilibrium processes. The thermodynamic data of proton pre-equilibrium were separately studied using the oxy-acids as adequate model of the RC. For proton uptake to a "normal" acid, including X−OH, the standard entropy change is positive ($T{\cdot}\Delta S_H^\circ$ = +184 meV > 0) and the pH dependence should appear as a negative entropy of mixing, $\Delta S_H^{\circ\prime}/d(pH) < 0$ leading to $T{\cdot}\Delta S_H^{\circ\prime}$ = −252 meV at pH 7.5 (Table 2). In contrast, for the second ET at pH 7.5, the apparent (total) activation entropy, $\Delta S_{tot}^{\#}$, is positive, and the slope, $d(\Delta S_{tot}^{\#})/d(pH)$, is substantially positive in almost all mutants except for WT and the singular L213DN mutant, which show slightly negative pH dependence (Tables 1−3). This indicates that the protonation equilibrium parameters are overwhelmed by the true activation parameters of the electron transfer (a Marcus-type expression), which must then have a large, negative $\Delta S_{ET}^{\#}$ and a substantial positive pH dependence in all strains except WT and the singular L213DN mutant.

In WT RC, the entropy change of the activation of the ET is positive ($T{\cdot}\Delta S_{ET}^{\#}$ = +70 meV), but the entropy increase is small relative to the enthalpy change of 270 meV. Additionally, the wild type has a substantially smaller relative enthalpy contribution than any other RC. Any manipulation of the proton pathway—by mutation or by divalent cations like Cd^{2+} or Ni^{2+}, which inhibit the capture and entry of protons into the proton conducting pathway[27]—results in a larger net enthalpy of activation and a less negative entropy. However, this partial offset is almost certainly not a significant "enthalpy−entropy compensation".[32,64] It is very unlikely that the ET step is intrinsically altered by these mutations and conditions, so this presumably corresponds to a progressive change in the non-ET modifier, from the rapid protonation pre-equilibrium to a rate limiting proton transfer (PT-limited).

For a significant group of RCs that are not ET-limited, the enthalpy increases and the entropy contribution becomes much less negative (Table 3). This includes all RCs in the presence of Ni^{2+}, which appears to be the most effective inhibitor of proton entry, and for the double mutants L210DN/M17DN, where the proton pathway is disrupted, and for L213DN/M44ND. However, it is not true for the single L213DN mutant, which is the most severely PT-limited of any created mutants by blocking the branching point of the proton pathway at a site nearer Q_B (Figure 1). The increase of the entropy is likely due to increasing contributions from the proton activation parameters, as this becomes rate limiting. When the reaction is distinctly PT-limited, as with Ni^{2+}, the activation process is almost entirely enthalpic at pH 7.5, but the pH dependence is strong and positive for both enthalpy and entropy. The positive slope suggests that H^+ binding, *per se*, may not be involved in the rate limiting step. It could, perhaps, be the formation of a hydrogen-bonded pathway, including solvent water, as has been well supported for carbonic anhydrase[58] and almost visualized in microbial

DOI: 10.1021/acs.jpcb.9b03506
J. Phys. Chem. B 2019, 123, 5463−5473

rhodopsins.[65] The positive pH dependence may reflect an increasing surface charge on the protein[66] and its influence on counterion binding and release due to the bonding rearrangements involved in establishing the proton conductive pathway. However, the dissimilar behavior of the L213DN mutant is remarkable and indicates a very different kind of limitation. The negative pH dependence of $\Delta S^{\#}_{tot}$ may show the requirement for H^+ binding in reaching the activated state.

CONCLUSIONS

We expect that the second electron transfer in bacterial RC serves as model system of coupled electron and proton transfer, and activation measurements performed in this study will be useful for checking the validity of models for proton-coupled electron transfer in other proteins or ion channels such as cytochrome oxidase or the water evolving system of green plants. Although the formal expansion of our results is clearly beyond the scope of this paper, a driving force assay would reveal the rate-limiting step in a supposed process and whatever the rate-limiting step may be, the measured free energy of activation must be in consonance with data presented in this paper.

AUTHOR INFORMATION

Corresponding Author

*(P.M.) Telephone: +36 62 544 120. Fax: +36 62 544 121. E-mail: pmaroti@sol.cc.u-szeged.hu.

ORCID

Péter Maróti: 0000-0003-2135-728X

Notes

The author declares no competing financial interest.

ACKNOWLEDGMENTS

I am grateful to Profs. James Smart (Department of Biological Sciences, University of Tennessee at Martin) for careful reading of the manuscript and Colin A. Wraight (deceased 2014) for the mutants and valuable suggestions and to Drs. Gábor Sipka (Biological Research Center Szeged, Hungary) and László Gerencsér for their contributions in the early phase of the work. The support from COST (CM1306) and EFOP-3.6.2-16-2017-0005 is acknowledged.

REFERENCES

(1) Wraight, C. A.; Intraprotein Proton Transfer − Concepts and Realities from the Bacterial Photosynthetic Reaction Center. In *Biophysical and Structural Aspects of Bioenergetics*; Wikstrom, M., Ed.; RSC Biomolecular Science Series; Royal Society of Chemistry: Cambridge, England, 2005; Chapter 12.

(2) Wraight, C. A. Chance and Design—Proton Transfer in Water, Channels and Bioenergetic Proteins. *Biochim. Biophys. Acta, Bioenerg.* **2006**, *1757*, 886−912.

(3) Reece, S. Y.; Nocera, D. G. Proton-coupled Electron Transfer in Biology: Results from synergistic Studies in Natural and Model Systems. *Annu. Rev. Biochem.* **2009**, *78*, 673−699.

(4) Stuchebrukhov, A. A. Redox-Driven Proton Pumps of the Respiratory Chain. *Biophys. J.* **2018**, *115* (5), 830−840.

(5) Checchetto, V.; Teardo, E.; Carraretto, L.; Formentin, E.; Bergantino, E.; Giacometti, G. M.; Szabo, I. Regulation of Photosynthesis by Ion Channels in Cyanobacteria and Higher Plants. *Biophys. Chem.* **2013**, *182*, 51−57.

(6) Stubbe, J.; Nocera, D. G.; Yee, C. S.; Chang, M. C. Radical Initiation in the Class I Ribonucleotide Reductase: Long-range Proton-coupled Electron Transfer? *Chem. Rev.* **2003**, *103* (6), 2167−2201.

(7) Hammes-Schiffer, S.; Soudackov, A. V. Proton-Coupled Electron Transfer in Solution, Proteins, and Electrochemistry. *J. Phys. Chem. B* **2008**, *112* (45), 14108−14123.

(8) Hammes-Schiffer, S.; Stuchebrukhov, A. A. Theory of Coupled Electron and Proton Transfer Reactions. *Chem. Rev.* **2010**, *110*, 6939−6960.

(9) Kretchmer, J. S.; Miller, T. F. Tipping the Balance between Concerted versus Sequential Proton-Coupled Electron Transfer. *Inorg. Chem.* **2016**, *55* (3), 1022−1031.

(10) Kaila, V. R. I. Long-range Proton-coupled Electron Transfer in Biological Energy Conversion: Towards Mechanistic Understanding of Respiratory Complex I. *J. R. Soc., Interface* **2018**, *15*, 20170916.

(11) Okamura, M. Y.; Paddock, M. L.; Graige, M. S.; Feher, G. Proton and Electron Transfer in Bacterial Reaction Centers. *Biochim. Biophys. Acta, Bioenerg.* **2000**, *1458*, 148−163.

(12) Wraight, C. A. Proton and Electron Transfer in the Acceptor Quinone Complex of Bacterial Photosynthetic Reaction Centers. *Front. Biosci., Landmark Ed.* **2004**, *9*, 309−327.

(13) Nabedryk, E.; Breton, J. Coupling of Electron Transfer to Proton Uptake at the Q_B Site of the Bacterial Reaction Center: a Perspective from FTIR Difference Spectroscopy. *Biochim. Biophys. Acta, Bioenerg.* **2008**, *1777* (10), 1229−1248.

(14) Maróti, P.; Govindjee. The Two Last Overviews by Colin Allen Wraight (1945−2014) on Energy Conversion in Photosynthetic Bacteria. *Photosynth. Res.* **2016**, *127* (2), 257−271.

(15) Maróti, P.; Wraight, C. A. Flash-induced H^+ Binding by Bacterial Photosynthetic Reaction Centers: Comparison of Spectrophotometric and Conductimetric Measurements. *Biochim. Biophys. Acta, Bioenerg.* **1988**, *934*, 314−328.

(16) Maróti, P. Chemical Rescue of H^+ Delivery in Proton Transfer Mutants of Reaction Center of Photosynthetic Bacteria. *Biochim. Biophys. Acta, Bioenerg.* **2019**, *1860*, 317−324.

(17) Paddock, M. L.; Feher, G.; Okamura, M. Y. Proton Transfer Pathways and Mechanism in Bacterial Reaction Centers. *FEBS Lett.* **2003**, *555*, 45−50.

(18) Maróti, Á.; Wraight, C. A.; Maróti, P. The Rate of Second Electron Transfer to Q_B^- in Bacterial Reaction Center of Impaired Proton Delivery Shows Hydrogen-isotope Effect. *Biochim. Biophys. Acta, Bioenerg.* **2015**, *1847*, 223−230.

(19) Maróti, Á.; Wraight, C. A.; Maróti, P. Protonated Rhodosemiquinone at the Q_B Binding Site of the M265IT Mutant Reaction Center of Photosynthetic Bacterium *Rhodobacter sphaeroides*. *Biochemistry* **2015**, *54* (12), 2095−2103.

(20) Graige, M. S.; Paddock, M. L.; Bruce, J. M.; Feher, G.; Okamura, M. Y. Mechanism of Proton-Coupled Electron Transfer for Quinone (Q_B) Reduction in Reaction Centers of Rb. *sphaeroides*. *J. Am. Chem. Soc.* **1996**, *118*, 9005−9016.

(21) Ädelroth, P.; Paddock, M. L.; Sagle, L. B.; Feher, G.; Okamura, M. Y. Identification of the Proton Pathway in Bacterial Reaction Centers: Both Protons Associated with Reduction of Q_B to Q_BH_2 Share a Common Entry Point. *Proc. Natl. Acad. Sci. U. S. A.* **2000**, *97*, 13086−13091.

(22) Xu, Q.; Axelrod, H. L.; Abresch, E. C.; Paddock, M. L.; Okamura, M. Y.; Feher, G. X-Ray Structure Determination of Three Mutants of the Bacterial Photosynthetic Reaction Centers from *Rb. sphaeroides*: Altered Proton Transfer Pathways. *Structure* **2004**, *12*, 703−715.

(23) Takahashi, E., Maróti, P.; Wraight, C. A. In *Electron and Proton Transfer in Chemistry and Biology*; Diemann, E., Junge, W., Müller, A., Ratazczak, H., Eds.; Elsevier: Amsterdam, 1992; pp 219−236.

(24) Paddock, M. L.; Ädelroth, P.; Chang, C.; Abresch, E. C.; Feher, G.; Okamura, M. Y. Identification of the Proton Pathway in Bacterial Reaction Centers: Cooperation between Asp-M17 and Asp-L210 Facilitates Proton Transfer to the Secondary Quinone (Q_B). *Biochemistry* **2001**, *40*, 6893−6902.

(25) Hanson, D. K.; Tiede, D. M.; Nance, S. L.; Chang, C.-H.; Schiffer, M. Site Specific and Compensatory Mutations Imply Unexpected Pathways for Proton Delivery to the Q_B Binding Site of

DOI: 10.1021/acs.jpcb.9b03506
J. Phys. Chem. B 2019, 123, 5463−5473

the Photosynthetic Reaction Center. *Proc. Natl. Acad. Sci. U. S. A.* **1993**, *90*, 8929−8933.
(26) Axelrod, H. L.; Abresch, E. C.; Paddock, M. L.; Feher, G.; Okamura, M. Y. Determination of the Binding Sites of the Proton Transfer Inhibitors Cd^{2+} and Zn^{2+} in Bacterial Reaction Centers. *Proc. Natl. Acad. Sci. U. S. A.* **2000**, *97*, 1542−1547.
(27) Gerencsér, L.; Maróti, P. Retardation of Proton Transfer Caused by Binding of the Transition Metal Ion to the Bacterial Reaction Center is Due to pK_a Shifts of Key Protonatable Residues. *Biochemistry* **2001**, *40*, 1850−1860.
(28) Xu, Q.; Gunner, M. R. Temperature Dependence of the Free Energy, Enthalpy, and Entropy of $P^+Q_A^-$ Charge Recombination in *Rhodobacter sphaeroides* R-26 Reaction Centers. *J. Phys. Chem. B* **2000**, *104*, 8035−8043.
(29) Edens, G. J.; Gunner, M. R.; Xu, Q.; Mauzerall, D. The Enthalpy and Entropy of Reaction for Formation of $P^+Q_A^-$ from Excited Reaction Centers of *Rhodobacter sphaeroides*. *J. Am. Chem. Soc.* **2000**, *122*, 1479−1485.
(30) Hou, H. J. M.; Shen, G.; Boichenko, V. A.; Golbeck, J. H.; Mauzerall, D. Thermodynamics of Charge Separation of Photosystem I in the menA and menB Null Mutants of Synechocystis sp. PCC 6803 Determined by Pulsed Photoacoustics. *Biochemistry* **2009**, *48*, 1829−1837.
(31) Onidas, D.; Sipka, G.; Asztalos, E.; Maróti, P. Mutational Control of Bioenergetics of Bacterial Reaction Center Probed by Delayed Fluorescence. *Biochim. Biophys. Acta, Bioenerg.* **2013**, *1827* (10), 1191−1199.
(32) Milano, F.; Dorogi, M.; Szebényi, K.; Nagy, L.; Maróti, P.; Váró, Gy.; Giotta, L.; Agostiano, A.; Trotta, M. Enthalpy/entropy Driven Activation of the First Interquinone Electron Transfer in Bacterial Photosynthetic Reaction Centers Embedded in Vesicles of Physiologically Important Phospholipids. *Bioelectrochemistry* **2007**, *70*, 18−22.
(33) Takahashi, E.; Wraight, C. A. A Crucial Role for AspL213 in the Proton Transfer Pathway to the Secondary Quinone of Reaction Centers from *Rhodobacter sphaeroides*. *Biochim. Biophys. Acta, Bioenerg.* **1990**, *1020*, 107−111.
(34) Takahashi, E.; Wraight, C. A. Potentiation of Proton Transfer Function by Electrostatic Interactions in Photosynthetic Reaction Centers from *Rhodobacter sphaeroides*: First Results from Site Directed Mutation of the H-subunit. *Proc. Natl. Acad. Sci. U. S. A.* **1996**, *93*, 2640−2645.
(35) Takahashi, E.; Wraight, C. A. Small Weak Acids Reactivate Proton Transfer in Reaction Centers from *Rhodobacter sphaeroides* Mutated at AspL210 and AspM17. *J. Biol. Chem.* **2006**, *281* (7), 4413−4422.
(36) Christensen, J. J.; Hansen, L. D.; Izatt, R. M. *Handbook of Proton Ionization Heats and Related Thermodynamic Quantities*; Wiley-Interscience, John Wiley & Sons: New York, 1976.
(37) Paddock, M. L.; Ädelroth, P.; Feher, G.; Okamura, M. Y.; Beatty, J. T. Determination of Proton Transfer Rates by Chemical Rescue: Application to Bacterial Reaction Centers. *Biochemistry* **2002**, *41*, 14716−14725.
(38) Eigen, M. Proton Transfer, Acid−Base Catalysis, and Enzymatic Hydrolysis. *Angew. Chem., Int. Ed. Engl.* **1964**, *3*, 1−19.
(39) Marcus, R. A.; Sutin, N. Electron Transfers in Chemistry and Biology. *Biochim. Biophys. Acta, Rev. Bioenerg.* **1985**, *811*, 265−322.
(40) Calvo, R.; Isaacson, R. A.; Paddock, M. L.; Abresch, E. C.; Okamura, M. Y.; Maniero, A. L.; Brunel, L. C.; Feher, G. EPR Study of the Semiquinone Biradical $Q_A^{\bullet-}Q_B^{\bullet-}$ in Photosynthetic Reaction Centers of *Rhodobacter sphaeroides* at 326 GHz: Determination of the Exchange Interaction J_o. *J. Phys. Chem. B* **2001**, *105* (19), 4053−4057.
(41) Graige, M. S.; Paddock, M. L.; Feher, G.; Okamura, M. Y. Observation of the Protonated Semiquinone Intermediate in Isolated Reaction Centers from *Rhodobacter sphaeroides*: Implications for the Mechanism of Electron and Proton Transfer in Proteins. *Biochemistry* **1999**, *38* (35), 11465−11473.
(42) Moser, C. C.; Keske, J. M.; Warncke, K.; Farid, R. S.; Dutton, P. L. Nature of Biological Electron Transfer. *Nature* **1992**, *355*, 796−802.
(43) Dutton, P. L.; Moser, C. C. Quantum Biomechanics of Long-range Electron Transfer in Protein: Hydrogen Bonds and Reorganization Energies. *Proc. Natl. Acad. Sci. U. S. A.* **1994**, *91*, 10247−10250.
(44) Martin, D. R.; Matyushov, D. V. Photosynthetic Diode: Electron Transport Rectification by Wetting the Quinone Cofactor. *Phys. Chem. Chem. Phys.* **2015**, *17* (35), 22523−22528.
(45) Meade, T. J.; Gray, H. B.; Winkler, J. R. Driving-force Effects on the Rate of Long-range Electron Transfer in Ruthenium-modified Cytochrome-*c*. *J. Am. Chem. Soc.* **1989**, *111*, 4353−4356.
(46) Crofts, A. R.; Guergova-Kuras, M.; Kuras, R.; Ugulava, N.; Li, J.; Hong, S. Proton-coupled Electron Transfer at the Q_o Site: What Type of Mechanism can Account for the High Activation Barrier? *Biochim. Biophys. Acta, Bioenerg.* **2000**, *1459*, 456−466.
(47) Allen, J. P.; Williams, J. C.; Graige, M.; Paddock, M. L.; Labahn, A.; Feher, G.; Okamura, M. Y. Free Energy Dependence of the Direct Charge Recombination from the Primary and Secondary Quinones in Reaction Centers from *Rhodobacter sphaeroides*. *Photosynth. Res.* **1998**, *55*, 227−233.
(48) Allen, J. P.; Williams, J. C. Photosynthetic Reaction Centers. *FEBS Lett.* **1998**, *438* (1−2), 5−9.
(49) Ortega, J. M.; Mathis, P.; Williams, J. C.; Allen, J. P. Temperature Dependence of the Reorganization Energy for Charge Recombination in the Reaction Center from *Rhodobacter sphaeroides*. *Biochemistry* **1996**, *35*, 3354−3361.
(50) Schmid, R.; Labahn, A. Temperature and Free Energy Dependence of the Direct Charge Recombination Rate from the Secondary Quinone in Bacterial Reaction Centers from *Rhodobacter sphaeroides*. *J. Phys. Chem. B* **2000**, *104*, 2928−2936.
(51) Franzen, S.; Boxer, S. G. Temperature Dependence of the Electric Field Modulation of Electron Transfer Rates: Charge Recombination in Photosynthetic Reaction Centers. *J. Phys. Chem.* **1993**, *97*, 6304−6318.
(52) Parson, W. W.; Chu, Z. T.; Warshel, A. Reorganization Energy of the Initial Electron-Transfer Step in Photosynthetic Bacterial Reaction Centers. *Biophys. J.* **1998**, *74*, 182−191.
(53) Calvo, R.; Passeggi, M. C.; Isaacson, R. A.; Okamura, M. Y.; Feher, G. Electron Paramagnetic Resonance Investigation of Photosynthetic Reaction Centers from *Rhodobacter sphaeroides* R-26 in which Fe^{2+} Was Replaced by Cu^{2+}. Determination of Hyperfine Interactions and Exchange and Dipole-Dipole Interactions between Cu^{2+} and Q_A^-. *Biophys. J.* **1990**, *58*, 149−165.
(54) Li, J.; Takahashi, E.; Gunner, M. R. $-\Delta G^\circ_{AB}$ and pH Dependence of the Electron Transfer from $P^+Q_A^-Q_B$ to $P^+Q_AQ_B^-$ in *Rhodobacter sphaeroides* Reaction Centers. *Biochemistry* **2000**, *39*, 7445−7454.
(55) Page, C. C.; Moser, C. C.; Chen, X.; Dutton, P. L. Natural Engineering Principles of Electron Tunnelling in Biological Oxidation-reduction. *Nature* **1999**, *402*, 47−52.
(56) Marcus, R. A. Theoretical Relations among Rate Constants, Barriers, and Brönsted Slopes of Chemical Reactions. *J. Phys. Chem.* **1968**, *72*, 891−899.
(57) Kresge, A. J. What Makes Proton Transfer Fast? *Acc. Chem. Res.* **1975**, *8*, 354−360.
(58) Silverman, D. N. Marcus Rate Theory Applied to Enzymatic Proton Transfer. *Biochim. Biophys. Acta, Bioenerg.* **2000**, *1458*, 88−103.
(59) Tu, Ch.; Qian, M.; Earnhardt, J. N.; Laipis, P. J.; Silverman, D. N. Properties of Intramolecular Proton Transfer in Carbonic Anhydrase III. *Biophys. J.* **1998**, *74*, 3182−3189.
(60) Chernyshev, A.; Cukierman, S. Thermodynamic View of Activation Energies of Proton Transfer in Various Gramicidin A Channels. *Biophys. J.* **2002**, *82*, 182−192.
(61) Schutz, C. N.; Warshel, A. Analyzing Free Energy Relationships for Proton Translocations in Enzymes: Carbonic Anhydrase Revisited. *J. Phys. Chem. B* **2004**, *108*, 2066−2075.

DOI: 10.1021/acs.jpcb.9b03506
J. Phys. Chem. B 2019, 123, 5463−5473

(62) Åqvist, J.; Kazemi, M.; Isaksen, G. V.; Brandsdal, B. O. Entropy and Enzyme Catalysis. *Acc. Chem. Res.* **2017**, *50*, 199−207.
(63) Åqvist, J.; Kamerlin, S. C. L. Exceptionally Large Entropy Contributions Enable the High Rates of GTP Hydrolysis on the Ribosome. *Sci. Rep.* **2015**, *5*, 15817.
(64) Khrapunov, S. The Enthalpy-entropy Compensation Phenomenon. Limitations for the Use of Some Basic Thermodynamic Equations. *Curr. Protein Pept. Sci.* **2018**, *19* (11), 1088−1091.
(65) Gerwert, K.; Freier, E.; Wolf, S. The Role of Protein-Bound Water Molecules in Microbial Rhodopsins. *Biochim. Biophys. Acta, Bioenerg.* **2014**, *1837*, 606−613.
(66) Maróti, P.; Wraight, C. A. Kinetics of H^+ Ion Binding by the $P^+Q_A^-$ State of Bacterial Photosynthetic Reaction Centers: Rate Limitation within the Protein. *Biophys. J.* **1997**, *73*, 367−381.

DOI: 10.1021/acs.jpcb.9b03506
J. Phys. Chem. B 2019, 123, 5463−5473